frontiers | Frontiers in Chemistry

TYPE Original Research
PUBLISHED 27 November 2023
DOI 10.3389/fchem.2023.1322475

OPEN ACCESS

EDITED BY
Xingjian Xue,
University of South Carolina,
United States

REVIEWED BY
Zetian Tao,
University of South China, China
Yun Gan,
Chemtronergy, LLC, United States

*CORRESPONDENCE
Muhammad Bilal Hanif,
hanif1@uniba.sk,
bilalhanif46@gmail.com
Martin Motola,
martin.motola@uniba.sk
Muneeb Irshad,
muneebirshad@gmail.com

RECEIVED 16 October 2023
ACCEPTED 16 November 2023
PUBLISHED 27 November 2023

CITATION
Ain Qu, Irshad M, Butt MS, Tabish AN, Hanif MB, Khalid MA, Ghaffar R, Rafique M, Shawar Kazmi SDE, Siraj K, Hafez AAA, Abd-Rabboh HSM, Zmrhalova Z, Filonova EA, Medvedev DA and Motola M (2023), Towards sustainable electrochemistry: green synthesis and sintering aid modulations in the development of $BaZr_{0.87}Y_{0.1}M_{0.03}O_{3-\delta}$ (M = Mn, Co, and Fe) IT-SOFC electrolytes.
Front. Chem. 11:1322475.
doi: 10.3389/fchem.2023.1322475

Towards sustainable electrochemistry: green synthesis and sintering aid modulations in the development of $BaZr_{0.87}Y_{0.1}M_{0.03}O_{3-\delta}$ (M = Mn, Co, and Fe) IT-SOFC electrolytes

Qurat ul Ain[1], Muneeb Irshad[1]*, Muhammad Salim Butt[2], Asif Nadeem Tabish[2,3], Muhammad Bilal Hanif[4,5]*, Muhammad Ali Khalid[6], Rabia Ghaffar[7], Muhammad Rafique[8], Syeda Dur E. Shawar Kazmi[1], Khurram Siraj[1], Amal A. Abdel Hafez[9], Hisham S. M. Abd-Rabboh[9], Zuzana Zmrhalova[10], Elena A. Filonova[11], Dmitry A. Medvedev[12,13] and Martin Motola[4]*

[1]Department of Physics, University of Engineering and Technology, Lahore, Pakistan, [2]Department of Electrical Engineering, University of Engineering and Technology, New Campus, Lahore, Pakistan, [3]Department of Chemical Engineering, University of Engineering and Technology, New Campus, Lahore, Pakistan, [4]Department of Inorganic Chemistry, Faculty of Natural Sciences, Comenius University Bratislava, Bratislava, Slovakia, [5]State Key Laboratory for Mechanical Behavior of Materials, School of Materials Science and Engineering, Xi'an Jiaotong University, Xi'an, Shaanxi, China, [6]State Key Laboratory of Multiphase Flow in Power Engineering, School of Energy and Power Engineering, Xi'an Jiaotong University, Xi'an, China, [7]Division of Science and Technology, Department of Botany, University of Education, Lahore, Pakistan, [8]Department of Physics, University of Sahiwal, Sahiwal, Pakistan, [9]Department of Chemistry, Faculty of Science, King Khalid University, Abha, Saudi Arabia, [10]Center of Materials and Nanotechnologies, Faculty of Chemical Technology, University of Pardubice, Pardubice, Czechia, [11]Institute of Natural Sciences and Mathematics, Ural Federal University, Ekaterinburg, Russia, [12]Hydrogen Energy Laboratory, Ural Federal University, Ekaterinburg, Russia, [13]Laboratory of Electrochemical Devices Based on Solid Oxide Proton Electrolytes, Institute of High Temperature Electrochemistry, Ekaterinburg, Russia

In this study, $BaZr_{0.87}Y_{0.1}M_{0.03}O_{3-\delta}$ perovskite electrolytes with sintering aids (M = Mn, Co, and Fe) were synthesized by a sustainable approach using spinach powder as a chelating agent and then compared with chemically synthesized $BaZr_{0.87}Y_{0.1}M_{0.03}O_{3-\delta}$ (M = Mn, Co, and Fe) electrolytes for intermediate temperature SOFCs. This is the first example of such a sustainable synthesis of perovskite materials with sintering aids. Structural analysis revealed the presence of a cubic perovskite structure in $BaZr_{0.87}Y_{0.1}M_{0.03}O_{3-\delta}$ (M = Mn, Co, and Fe) samples synthesized by both green and conventional chemical methods. No significant secondary phases were observed in the samples synthesized by a sustainable approach. The observed phenomena of plane shift were because of the disparities between ionic radii of the dopants, impurities, and host materials. The surface morphology analysis revealed a denser microstructure for the electrolytes synthesized via green routes due to metallic impurities in the organic chelating agent. The absence of significant impurities was also observed by compositional analysis, while functional groups were identified through Fourier-transform infrared spectroscopy. Conductivity measurements showed that $BaZr_{0.87}Y_{0.1}M_{0.03}O_{3-\delta}$ (M = Mn, Co, and Fe) electrolytes synthesized by oxalic acid have higher conductivities compared to $BaZr_{0.87}Y_{0.1}M_{0.03}O_{3-\delta}$ (M = Mn, Co, and Fe) electrolytes synthesized by

the green approach. The button cells employing $BaZr_{0.87}Y_{0.1}Co_{0.03}O_{3-\delta}$ electrolytes synthesized by the chemical and green routes achieved peak power densities 344 and 271 $mW{\cdot}cm^{-2}$ respectively, suggesting that the novel green route can be applied to synthesize SOFC perovskite materials with minimal environmental impact and without significantly compromising cell performance.

KEYWORDS

perovskite, green synthesis, SOFC, proton conductor, barium zirconate, electrochemical performance

1 Introduction

Energy is a crucial element in the long-term development and wellbeing of all nations. As the world's population has grown and technological industrialization has progressed, energy has become an indispensable requirement for daily life. Energy consumption is also essential for economic development and prosperity, especially for electricity generation and industrial use (Babar et al., 2022; Hanif et al., 2023a; Antonova, 2023; Gordeev and Porotnikova, 2023; Shaheen et al., 2023). Fossil fuels are still the primary sources of energy but concerns about greenhouse gas emissions and climate change have increased, forcing the world to explore renewable and sustainable energy sources (Hanif et al., 2022; Irshad et al., 2022; Demin and Bronin, 2023; Pikalova et al., 2023). Fuel cells, particularly solid oxide fuel cells (SOFCs), have become prominent contenders amongst alternative energy sources because of their efficiency, ability to use multiple fuels, and little or no greenhouse gas emissions (Rafique et al., 2022; Hanif et al., 2023b; Khan et al., 2023; Rauf et al., 2023; Tarasova et al., 2023; Babar et al., 2024). In the last decade, special attention has been focused on proton-conducting SOFCs owing to their high protonic conductivity compared to oxygen conduction because of the small size of protons with their low activation energy (Irshad et al., 2023; Mehran et al., 2023).

The electrolyte is an essential component of SOFCs, and its improvements are critical in reducing operating temperatures and achieving good chemical stability and ionic conductivity at the same time. Many ionic conductors, including YSZ, doped gallates and doped CeO_2, etc., are investigated as SOFC electrolytes. Nevertheless, these electrolytes need a substantial amount of activation energy and elevated temperature in order to achieve good conductivity. Proton conductors have the potential to be suitable for use as electrolytes due to their favorable proton conductivity at low temperatures (Irshad et al., 2016; Mosiałek et al., 2023). Perovskite materials (ABO_3) have attracted considerable attention as electrolyte materials because they can surpass the constraints of traditional electrolytes. The highly conducting perovskite electrolytes can transport ions more efficiently across the material. The aforementioned attribute can enhance the SOFC performance device by facilitating swift ions transport and minimizing resistances. In addition, these electrolytes are also more stable than conventional electrolytes in reductive/oxidative atmospheres at high operating temperatures (Irshad et al., 2023).

Doped barium zirconate ($BaZrO_3$) and barium cerate ($BaCeO_3$) are commonly used proton conducting electrolytes based on the perovskite structure (ABO_3). Doped $BaCeO_3$exhibits high conductivity, however it lacks chemical stability in CO_2 and humid atmospheres, whereas doped $BaZrO_3$ exhibits high stability in these atmospheres, but have lower ionic conductivity (Goulart et al., 2021; Rasaki et al., 2021; Zhang and Hu, 2021). Various sintering aids, synthesis routes and doping approaches are used to increase the density and conductivity of barium zirconate-based materials (Jiao et al., 2019). Introducing rare earth elements to the B-site creates oxygen vacancies, which in turn enhances ionic conductivity. Consequently, perovskites doped with rare earth (RE) elements have garnered interest because of their elevated levels of ionic, proton, or mixed conductivities (Irshad et al., 2021; Rasaki et al., 2021). The addition of dopants in perovskites and especially in $BaZrO_3$ enhances the proton mobility and therefore boosts proton conductivity at intermediate temperatures (Nayak and Sasmal, 2023). The meticulous choice of dopants along with fabrication techniques could ascertain the effective formation of conductive and stable $BaZrO_3$-based electrolytes (Hossain et al., 2021a). RE-doped $BaZrO_3$ exhibit significant protonic conductivity at low temperatures making them a suitable choice. However, there are still existing problems, such as the limited ability of protons to be absorbed and the insufficient number of catalytic sites which needs to be addressed. Furthermore, achieving dense $BaZrO_3$-based electrolytes necessitates elevated sintering temperature and prolonged sintering duration. High sintering temperatures results in evaporation of BaO, causing a decrease in grain and grain boundary conductivity due to ternary phase formation (Ueno et al., 2019). Also, $BaZrO_3$ has a grain boundary blocking property caused by a space charge effect which segregates the charged defects near structurally distorted region of the grain boundary (Uthayakumar et al., 2020). Despite substantial research on the proton conduction of doped $BaZrO_3$, the exact processes underlying the conduction of doped $BaZrO_3$ is remain poorly understood (Vera et al., 2021). It is however an established fact that synthesis approaches, selection of dopants and sintering aids are crucial role for promoting the desired properties of RE-$BaZrO_3$ materials (Hossain et al., 2021b).

Researchers have reported the use of sintering aids to decrease the sintering temperature while upholding the attributes of the SOFC materials. Soares et al. (2021) investigated ZnO as a sintering aid with different stoichiometric ratios in $Ba(Zr,Y)O_{3-\delta}$ to improve the densification, bulk proton conductivity, and high hydration enthalpy. Ho-Il Ji et al. investigated 1 and 4 mol% of CuO and ZnO as sintering aids to reduce the sintering temperature from 1,700°C to 1,500°C and 1,300°C, respectively and achieved relative densities above 97% (Ji et al., 2021). The use of transition metals (Sc, Zn, Co, Cu, and Fe, etc.) as co-dopants can improve the sinterability and thus increase the densification (Xie et al., 2018; Ueno et al., 2019;

Aarthi and Babu, 2020). Xie et al. (2018) observed the co-doing effect of Gd-Zn on barium zirconate sintered at 1,300°C–1,500°C, which improved the mechanical performance, sinterability, hardness, and conductivity, achieving a conductivity of 2.54×10^{-3} S·cm^{-1} and power density of 282 mW·cm^{-2}.

Diverse synthetic pathways, encompassing both physical and chemical methodologies, have been utilized to synthesize of SOFC materials. However, these procedures have a substantial ecological impact (Zheng et al., 2009; Zhang and Hu, 2021; Tong et al., 2022). Little or no effort has been made to synthesize perovskite SOFC materials by green synthesis due to the presence of organic and inorganic impurities that significantly hinder or degrade the performance of SOFCs. Spinach was used as a chelating agent to leverage the synergistic role of both its biomolecules and natural oxalic acid (present in high content) as a reducing and capping agent. Furthermore, the metallic impurities it contains might act as a sintering aid, resulting in the better densification at a lower sintering temperature. Spinach is frequently associated with a high oxalic acid concentration, with a quantity of around 3.45 ± 0.22 mg·g^{-1} (Uwah et al., 2011). The metal content in spinach is Zn, 6.10 ± 0.12; Mn, 10.50 ± 0.90; As, 0.90 ± 0.26; Pb, 2.40 ± 0.16; Cu, 0.88 ± 0.07 and Cd, 0.26 ± 0.02 µg·g^{-1} (Osinkin, 2023). Furthermore, there is no literature to date where perovskite materials with sintering aids have been developed by green synthesis. In the current project, a novel sustainable approach will be developed to synthesize the perovskite materials with sintering aids using biomolecules and natural chelating agents as reducing and capping agents with minimal impurities. $BaZr_{0.87}Y_{0.1}M_{0.03}O_{3-\delta}$ perovskite electrolytes co-doped with sintering aids (M = Co, Fe, Mn) have been successfully synthesized via green and chemical routes using bio- and chemical chelating agents respectively. The $BaZr_{0.87}Y_{0.1}M_{0.03}O_{3-\delta}$ (M = Co, Fe, Mn) samples synthesized with oxalic acid is denoted as BZYCo (OA), BZYFe (OA), and BZYMn (OA), respectively. Similarly, the $BaZr_{0.87}Y_{0.1}M_{0.03}O_{3-\delta}$ (M = Co, Fe, Mn) samples synthesized with spinach is labeled as BZYCo (SP), BZYFe (SP), and BZYMn (SP), respectively.

2 Experimentation

$BaZr_{0.87}Y_{0.1}M_{0.03}O_{3-\delta}$ (BZYM) with transition metal as B-site co-dopants (M = Co, Fe, Mn) were synthesized by auto-combustion method using different chelating agents, i.e., oxalic acid and spinach dried leaves powder. The stoichiometric amount of $[Ba(NO_3)_2]$, $[Zr(NO_3)_4{\cdot}5H_2O]$, $[Y(NO_3)_3{\cdot}6H_2O]$, $[Mn(NO_3)_2{\cdot}2H_2O]$, $[Fe(NO_3)_3{\cdot}9H_2O]$ and $[Co(NO_3)_2{\cdot}6H_2O]$ were dissolved in distilled water on a hot plate with a magnetic stirrer at 80°C for 30 min and then stirred at 120°C for 60 min to obtain a homogeneous solution. 20 wt.% of oxalic acid was dissolved in the homogeneous solution as a chelating agent. The solution was stirred continuously at 90°C to form a gel which was auto combusted to powder form. The powder obtained was sintered at 1,180°C for 6 h. The same stoichiometric amount of nitrate was used to prepare another homogeneous solution in the same way, with another chelating agent, i.e., 20 wt.% of spinach dry leaves powder. Again, the homogeneous solution was stirred at 80°C for 30 min and then stirred at 120°C for 60 min to produce a gel that auto combusted into powder. These powder samples were also sintered at 1,180°C for 6 h. The pellets were formed using a hydraulic press at 100 MPa for 5 min (Figure 1).

2.1 Material characterizations

The analysis of the $BaZr_{0.87}Y_{0.1}M_{0.03}O_{3-\delta}$ (M = Co, Fe, Mn) was conducted through X-Ray diffractometer (XRD; Bruker D8, Netherlands), Thermogravimetric analysis (TGA; STA 449 F5 Jupiter, Netzsch, Selb, Germany), Scanning electron microscopy (FESEM JEOL, Japan), Energy dispersive analysis (EDX), Fourier Transform Infrared spectroscopy (FTIR; JASCO 4600). The ionic conductivity was obtained through four probe DC method at 200°C–600°C. Ionic conductivity was calculated using equation.

$$\sigma = L/RA \tag{1}$$

The Arrhenius equation was used to determine the relation between temperature and conductivity.

$$\sigma = \sigma_{\circ} \exp\left(-E_a/KT\right) \tag{2}$$

2.2 Cell fabrication

The electrochemical performances of BZYM (M = Co, Fe, Mn) electrolytes, utilizing oxalic acid and spinach powder as chelating agents, were assessed. Pellets with a diameter of 13 mm and a thickness of 0.6 mm were prepared using a hydraulic press under a pressure of 200 MPa. BSCF and Ni-BZY were used as cathode and anode with $BaZr_{0.87}Y_{0.1}M_{0.03}O_{3-\delta}$ (M = Co, Fe, Mn) as electrolyte for the electrochemical measurements of the button cell. Humidified (~3% H_2O) hydrogen is supplied as fuel at the anode at 50 mL·min^{-1} while oxygen is supplied as an oxidant at the cathode.

3 Results and discussion

3.1 Crystal structure analysis

Figures 2A, B shows the XRD spectra of BZYM (M = Co, Fe, Mn) perovskite electrolyte, synthesized through chemical and green routes. The presence of diffraction peaks at (110), (111), (200), (211), (220), and (310) provides confirmation that all BZYM electrolytes exhibit a cubic perovskite structure and belongs to the primitive space group *Pm3m* (ICDD# 98 010 7880) (Jiao et al., 2019). The absence of significant secondary phases of zirconium, yttrium, or transition metals confirms single cubic perovskite structure. The lack of subsequent phases also confirms the solubility of transition metals (Mn, Fe, Co) in the host lattice synthesized by both chemical and green synthesis methods.

The orientation of the plane (110) corresponds to the alteration in lattice parameter, resulting in either an increase (cell volume expansion) or reduction (cell volume contraction) depending on the ionic radii and dopant concentration (Irshad et al., 2021). BZY shows a peak shift to a lower angle compared to the pure barium zirconate, which has an intense diffraction peak at $2\Theta = 30^{\circ}$, because

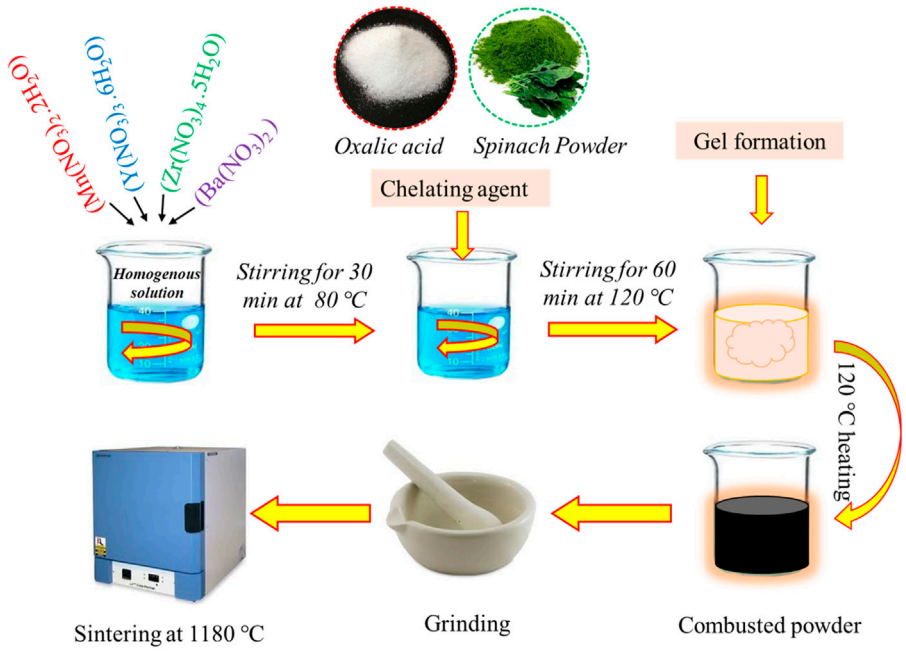

FIGURE 1
Schematic representation for the synthesis of $BaZr_{0.87}Y_{0.1}M_{0.03}O_{3-\delta}$ (BZYM) electrolyte.

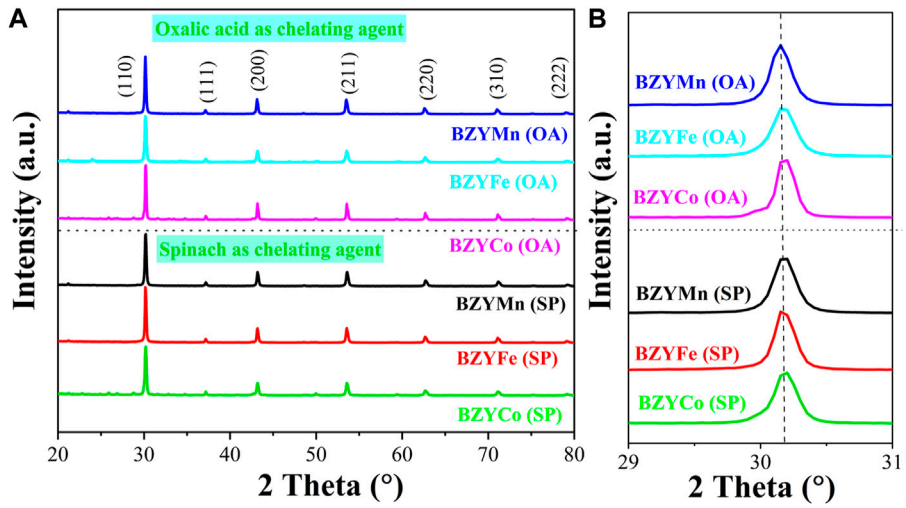

FIGURE 2
XRD spectra of BZYM (M = Co, Fe, Mn) electrolytes synthesized by chemical (oxalic acid) and green (spinach) routes **(A)** and enlarged (110) plane **(B)**.

of disparity between ionic radii of host (r = 0.72 Å for $Zr^{+4}{}_{VI}$) and dopant (for $Y^{+3}{}_{VI}$ r = 0.9 Å) (Ueno et al., 2019; Vera et al., 2021; Irshad et al., 2022). In our case, this peak shift occurs at $2\Theta = 30.15^{o}$ for (110) plane of BZYCo (OA), BZYFe (OA), BZYMn (OA), BZYCo (SP), BZYFe (SP) and BZYMn (SP). This shift of the peak to a higher angle compared to BZY, indicating lattice contraction due to the incorporation of small ionic radii of secondary dopants, i.e., $Co^{+3}{}_{VI(HS)}$ (0.61 Å), $Fe^{+3}{}_{VI(HS)}$ (0.65 Å), and $Mn^{+3}{}_{VI(HS)}$ (0.66 Å) into BZY compared to the host element Zr (0.72 Å) and dopant Y (0.9 Å). The crystallite sizes of BZYCo (OA), BZYFe (OA), BZYMn (OA), BZYCo (SP), BZYFe (SP) and BZYMn (SP) were calculated using the Scherer formula as follows:

$$D = \frac{K\lambda}{\beta \cos \Theta} \tag{3}$$

The crystallite sizes of the synthesized materials BZYM (M = Co, Fe, Mn) with chemical and green routes are given in Table 1.

3.2 Surface morphological analysis

Figures 3A–F show the SEM micrographs of the synthesized BZYM (M = Co, Fe, Mn) using spinach and oxalic acid as chelating agents respectively. It is clear that all the synthesized materials have a dense microstructure. However, BZYM (M = Co, Fe) synthesized by the green route are slightly denser compared to BZYM (M = Co, Fe) synthesized by the chemical approach which is attributable to low concentration of metallic impurities present in the spinach powder, which acts as a sintering aid and leads to increased densification. The BZYMn electrolyte on the other hand shows an opposite trend, with BZYMn synthesized by the green route, resulting in slightly lower densification than the material synthesized by the chemical route due to high concentration of Mn that already exist in spinach resulting in the slightly lower densification (Irshad et al., 2022). The overall densification order for BZYM (M = Co, Fe, Mn) electrolytes synthesized by both green and chemical routes can be represented as BZYMn < BZYFe < BZYCo indicating that Co doping acted as a slightly better sintering aid compared to Fe and Mn because Co doping can help to control the grain growth resulting in a fine-grained microstructure, as can also be seen from the micrographs too (Rehman et al., 2021).

TABLE 1 Average crystallite size of BZYM (M = Co, Fe, Mn) electrolytes synthesized with oxalic acid (OA) and spinach dry leaves powder (SP) as chelating agents.

Material	Dopant	Average crystallite size (nm)
BZYCo (OA)	Co	25
BZYFe (OA)	Fe	28
BZYMn (OA)	Mn	29
BZYCo (SP)	Co	23
BZYFe (SP)	Fe	26
BZYMn (SP)	Mn	30

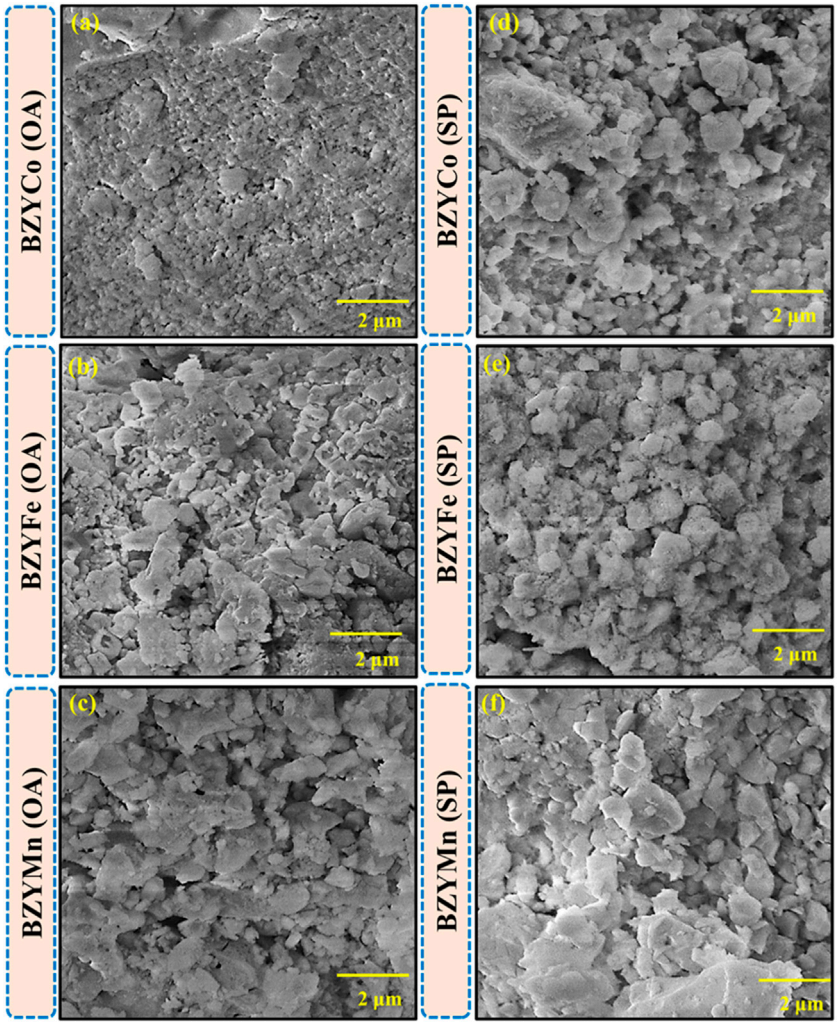

FIGURE 3
Surface morphology of BZYM (M = Co, Fe, Mn) electrolytes synthesized by green **(A–C)** and chemical routes **(D–F)**.

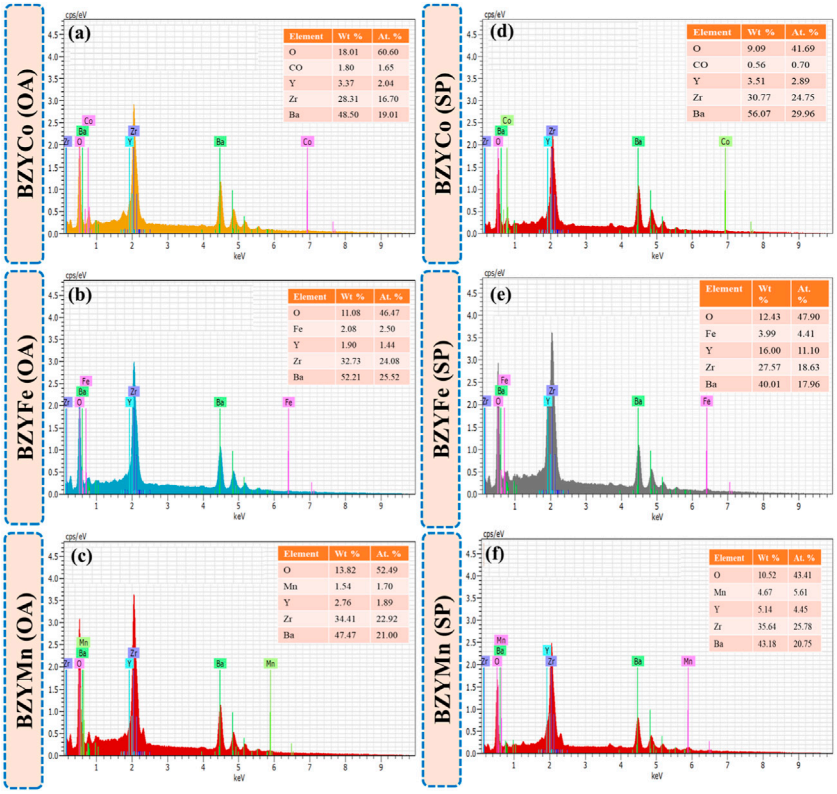

FIGURE 4
EDS qualitative with quantitative inset analysis of BZYM (M = Co, Fe, Mn) electrolytes using green **(A–C)** and chemical **(E–F)** route.

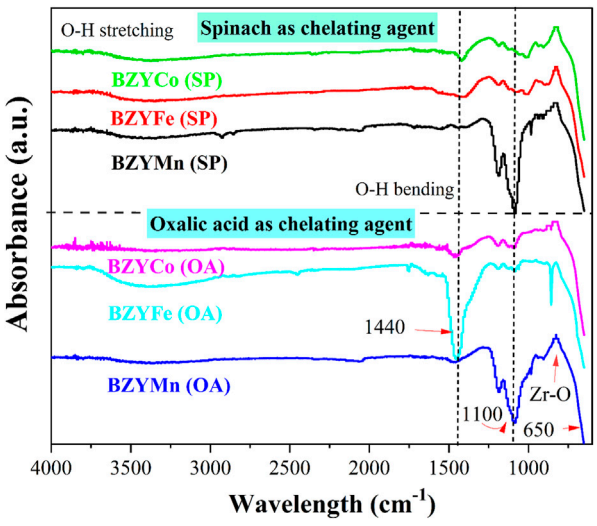

FIGURE 5
FTIR spectra of BZYM (M = Co, Fe, Mn) electrolytes synthesized by green and chemical route.

3.3 Elemental composition analysis

Figures 4A–F show the EDS spectra of sintered BZYM (M = Co, Fe, Mn) perovskite electrolytes synthesized using spinach and oxalic acid. The compositional analysis of BZYM (M = Co, Fe, Mn) confirms the presence of Ba, Zr, Y, and transition metal dopants (Co, Fe, Mn). The insets in Figures 4A–F show the quantitative analysis of BZYM (M = Co, Fe, Mn) for oxalic acid and spinach powder. It can be observed that no significant impurities were present in BZYM (M = Co, Fe, Mn) synthesized by the green route implying that spinach can be successfully used as chelating agent for the synthesis of $BaZr_{0.87}Y_{0.1}M_{0.03}O_{3-\delta}$ electrolyte without any significant impurities.

3.4 Spectroscopic analysis

Figure 5 presents the FTIR spectra of BZYM (M = Mn, Co, and Fe) perovskite electrolytes synthesized through chemical and green routes. The absorption bands at 3,800–3,200 cm^{-1} and 1700–1,400 cm^{-1} correspond to OH stretching and bending, respectively. These bands indicate the incorporation of water into the lattice which may be due to the atmospheric humidity (moisture). The peaks at 1,500–1,100 cm^{-1} indicate the formation of metal-oxygen-metal bonds such as Ba–O–Ba, Mn–O–Mn, Fe–O–Fe, etc. For Fe-doped BZY, broad and high intensity peaks in the 1,500–1,400 cm^{-1} region are characteristic of Fe–O bond formation (Jincy and Meena, 2022). The intensity of BZYFe electrolyte synthesized with oxalic acid is greater compared to BZYFe electrolyte synthesized with spinach powder, indicating the increased structural disorder (Irshad et al., 2022). The Mn-

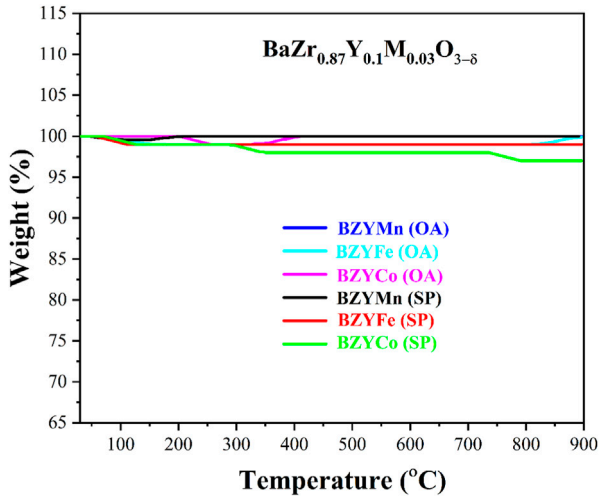

FIGURE 6
Thermogravimetric curves for BZYM (M = Co, Fe, Mn) electrolytes synthesized by chemical and green route.

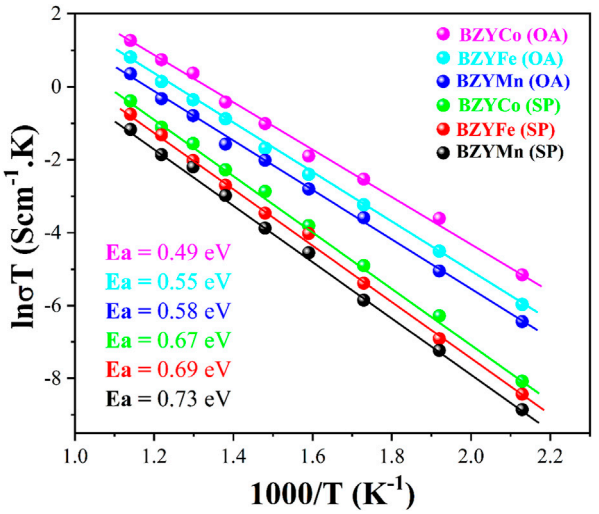

FIGURE 7
Arrhenius plot of BZYM (M = Co, Fe, Mn) electrolytes synthesized by chemical and green route.

doped BZY for both chelating agents shows an intense absorption peak at about 1,100 cm^{-1} which is characteristic of Mn–O bond formation. The absorption peak at about 1,200 cm^{-1} indicates C–O stretching. The absorption bands at 400–800 cm^{-1} indicate stretching vibrations of metal-oxygen bonds such as Mn–O, Fe–O, etc. The presence of metal-oxide bond peaks confirms the formation of transition metal doped BZY for both chemical and green synthesis routes.

3.5 Thermal analysis

Figure 6 shows the thermal analysis of sintered BZYM (M = Co, Fe, Mn) perovskite electrolyte. The TGA graph shows the weight loss in % over the temperature range 30°C–900°C. A minimal amount of weight loss is observed as the TGA was performed after sintering. The process of sintering has already removed the residual water and decomposed the nitrates and other organic impurities. Small weight losses of about 1%–3% may occur due to the incorporation of moisture or impurities into the synthesized materials after sintering. It can be inferred from no prominent weight loss that the BZYM (M = Co, Fe, Mn) electrolytes synthesized through chemical and green routes are thermally stable in the solid oxide fuel cell operating temperature range.

3.6 Conductivity

Figure 7 shows the Arrhenius plot for the BZYM (M = Co, Fe, Mn) perovskite electrolytes synthesized with chemical and organic chelating agents. It can be seen from the plot that regardless of the synthesis approach and dopants, all electrolytes exhibited significant conductivities which can be attributed to the fact that the addition of Co, Fe and Mn as the sintering aids lowers the sintering temperature and enhances the p-type conductivity as previously reported (Park et al., 2015).

It is clear from the plot that BZYCo (OA), BZYFe (OA) and BZYMn (OA) electrolytes showed better conductivity compared to electrolytes synthesized with spinach as a chelating agent. The lower conductivity of the BZYCo (SP), BZYFe (SP) and BZYMn (SP) electrolytes can be attributed to metallic impurities present in the spinach and the synergistic effect of both these impurities and dopants (M = Co, Fe, Mn) may have resulted in the lower ionic conductivity of the electrolytes, as these metals reduce the effective concentration of protons, acting as a proton trap, residing on the tetravalent Zr sites. It is well known that the conductivity of the electrolytes in air is attributed to electron-hole conduction and therefore the presence of these metals will result in a lower ionic conductivity (Tao and Irvine, 2007; Park et al., 2015). Nevertheless, the inclusion of sintering aids in the BZY solid solutions elevates the vacancy concentration of oxygen and barium sites, as previously stated (Huang et al., 2010; Benamira et al., 2011). It can also be observed from the plot that BZYCo (OA) and BZYCo (SP) exhibit high conductivity, because Co doping develops oxygen vacancies by replacing Zr at the B-site and these vacancies allow for faster oxygen ion transport, therefore resulting in higher ionic conductivity (Balaguer et al., 2022). The activation energies of the BZYCO (OA), BZYFe (OA) and BZYMn (OA) are 0.49, 0.55, and 0.58 eV respectively, while those of BZYCO (SP), BZYFe (SP) and BZYMn (SP) are 0.67, 0.69, and 0.73 eV respectively. The oxalic acid was used in the pure chemical form without any impurities as a reducing agent, however, spinach uses both oxalic acid (present in higher content) and biomolecules as a reducing and capping agent. Furthermore, spinach also carries metallic impurities that may act as a sintering aid along with a change in electrical properties causing a change in the activation energies compared to chemically synthesized BZYM electrolytes. It indicates that BZYM can be successfully used as an electrolyte despite the presence of impurities in the organic chelate.

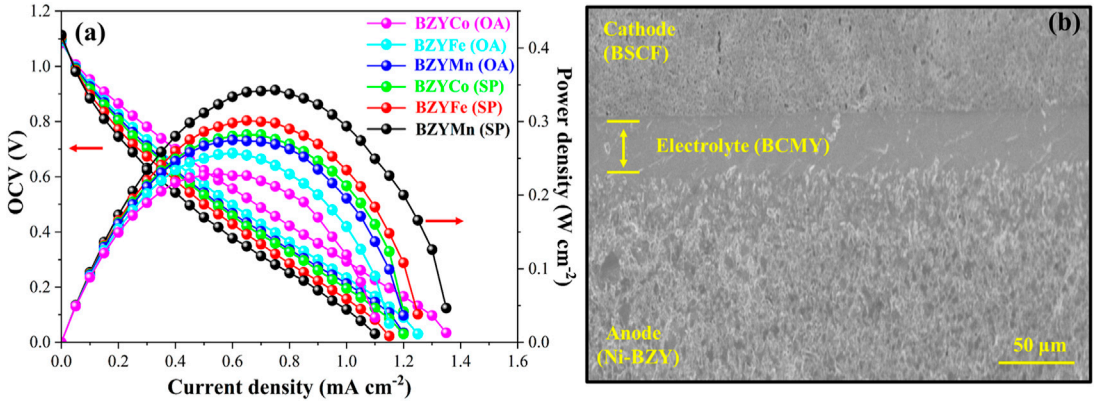

FIGURE 8
Electrochemical performance of cells at 650°C with BZYM (M = Co, Fe, Mn) electrolytes synthesized by green and chemical route **(A)**; along with the cross-sectional SEM images of anode supported cell (Ni-BZY | BCYM | BSCF) **(B)**.

3.7 Electrochemical performance

The electrochemical performance at 650°C for button cells with BZYM (M = Co, Fe, Mn) electrolytes synthesized through chemical and green routes is shown in Figure 8A. The maximum power densities of 344, 293, and 282 mW·cm^{-2} were achieved for the cells with the BZYCO (OA), BZYFe (OA) and BZYMn (OA) respectively. While cells with the BZYCO (SP), BZYFe (SP) and BZYMn (SP) electrolytes, exhibited power densities of 271, 265, and 218 mW·cm^{-2}, respectively, indicating that BZYM (M = Co, Fe, Mn) synthesized by both routes can be used as IT-SOFC electrolytes. It can be observed that the obtained power densities are lower than some of the reported values and can be ascribed to the low sintering temperature than the reported sintering temperatures. It is also clear that cells having BZYCo electrolytes synthesized with both routes shows higher power density compared to BZYFe and BZYMn synthesized with corresponding synthesis routes which can be attributed to its dense structure as seen from the surface morphology and the development of oxygen vacancies by replacing the Zr at the B-site, thus resulting in better performance (Gao et al., 2023).

It can be further observed from Figure 8A that the BZYCO (SP), BZYFe (SP) and BZYMn (SP) electrolytes exhibited low power densities compared to the BZYCO (OA), BZYFe (OA) and BZYMn (OA) electrolytes which can be linked to metallic impurities present in spinach causing the formation of structural defects that alter the electrical properties and hence the performance. However, extensive investigation and optimization is still required to fully understand the mechanism that affects the properties of the electrolytes due to metallic impurities present in the organic. Figure 8B shows the cross-sectional SEM images of the anode-supported half-button cell, utilizing BSCF and Ni-BZY as the cathode and anode, respectively. The cross-section reveals a densely structured electrolyte with a well-established connection between the anode and the electrolyte. Overall, it can be concluded that BZYM (M = Co, Fe, Mn) synthesized via sintering aids using this sustainable approach can be successfully used as IT-SOFC electrolytes.

4 Conclusion

In summary, for the first time a sustainable approach is successfully employed to synthesize BZYM perovskite electrolytes with sintering aids (Co, Fe, Mn) using spinach without significantly compromising its properties as an electrolyte for SOFC applications. The cubic perovskite structure was confirmed by the XRD with no prominent secondary phases, while the plane shift was due to mismatched ionic radii of dopants, host and impurities. The compositional study confirmed the existence of Ba, Zr and Y together with their respective sintering aids in each sample. Surface micrographs revealed a dense microstructure for all synthesized materials with slight differences in morphology, while the formation of a perovskite structure was also confirmed by the FTIR. The chemically synthesized BZYM (M = Co, Fe, Mn) electrolytes exhibited higher conductivities compared to the green synthesized BZYM (M = Co, Fe, Mn) electrolytes with $BaZr_{0.87}Y_{0.1}M_{0.03}O_{3-\delta}$ (M = Co) electrolytes exhibiting the highest conductivity in both cases. The maximum power density of 271 mW·cm^{-2} is attained for the cell having BZYCo electrolyte synthesized by the sustainable approach, suggesting the effective application of this innovative approach in synthesizing perovskite SOFC electrolytes.

Data availability statement

The raw data supporting the conclusion of this article will be made available by the authors, without undue reservation.

Author contributions

QA: Conceptualization, Data curation, Investigation, Methodology, Writing–original draft, Writing–review and editing. MI: Conceptualization, Data curation, Formal Analysis, Funding acquisition, Investigation, Methodology, Project administration, Resources, Software, Supervision, Validation, Visualization, Writing–original draft, Writing–review and editing. MB: Formal Analysis, Investigation, Methodology, Writing–review and editing. AT: Conceptualization, Formal Analysis, Investigation, Methodology, Writing–review and editing. MH: Conceptualization, Data curation, Investigation, Methodology, Project administration, Resources, Supervision, Visualization, Writing–original draft. MK: Formal Analysis, Investigation, Validation, Visualization, Writing–review and editing. RG: Formal Analysis, Investigation, Methodology, Writing–review and editing. MR: Investigation, Validation, Writing–review and editing. SS: Formal Analysis, Investigation, Methodology, Writing–review and editing. KS: Formal Analysis, Investigation, Methodology, Writing–review and editing. AH: Data curation, Formal Analysis, Funding acquisition, Investigation, Writing–review and editing. HA-R: Funding acquisition, Investigation, Methodology, Validation, Visualization, Writing–review and editing. ZZ: Formal Analysis, Investigation, Methodology, Writing–review and editing. EF: Conceptualization, Formal Analysis, Funding acquisition, Investigation, Methodology, Validation, Visualization, Writing–original draft, Writing–review and editing. DM: Conceptualization, Formal Analysis, Investigation, Methodology, Validation, Visualization, Writing–review and editing. MM: Formal Analysis, Investigation, Methodology, Resources, Validation, Visualization, Writing–review and editing.

Funding

The authors declare financial support was received for the research, authorship, and/or publication of this article. The authors extend their appreciation to the Deanship of Scientific Research at King Khalid University for funding this work through the Large Groups Project under grant number (RGP.2/335/44).

Conflict of interest

The authors declare that the research was conducted in the absence of any commercial or financial relationships that could be construed as a potential conflict of interest.

Publisher's note

All claims expressed in this article are solely those of the authors and do not necessarily represent those of their affiliated organizations, or those of the publisher, the editors and the reviewers. Any product that may be evaluated in this article, or claim that may be made by its manufacturer, is not guaranteed or endorsed by the publisher.

References

Aarthi, U., and Babu, K. S. (2020). Grain boundary space charge modulation in BaZr0. 8Y0. 2-xMxO3− δ with transition metal (M= Ni, Co, Fe, and Zn) co-doping. *Int. J. Hydrogen Energy* 45 (53), 29356–29366. doi:10.1016/j.ijhydene.2020.07.207

Antonova, E. P. (2023). Proton-conducting oxides based on $LaScO_3$: structure, properties and electrochemical applications. A focus review. *Electrochem. Mater. Technol.* 2 (4), 20232021. doi:10.15826/elmattech.2023.2.021

Babar, Z. U. D., Hanif, M. B., Gao, J.-T., Li, C.-J., and Li, C.-X. (2022). Sintering behavior of BaCe0.7Zr0.1Y0.2O3-δ electrolyte at 1150 °C with the utilization of CuO and Bi2O3 as sintering aids and its electrical performance. *Int. J. Hydrogen Energy* 47, 7403–7414. doi:10.1016/j.ijhydene.2021.12.075

Babar, Z. U. D., Hanif, M. B., Lin, X. L., Gao, J., Mosiałek, M., and Li, C. X. (2024). Design of a highly stable and conductive electrolyte by suppressing barium copper oxide formation at the grain interfaces in Cux-doped BaCe0.7Zr0.1Dy0.2-xO3-δ sintered at a low temperature (1200 °C) for SOFCs. *J. Colloid Interface Sci.* 654, 1124–1135. doi:10.1016/j.jcis.2023.10.094

Balaguer, M., Sohn, Y. J., Kobertz, D., Kasatikov, S., Fantin, A., Müller, M., et al. (2022). Characterization of Y and Mn co-substituted BaZrO3 ceramics: material properties as a function of the substituent concentration. *Solid state ionics* 382, 115959. doi:10.1016/j.ssi.2022.115959

Benamira, M., Ringuedé, A., Albin, V., Vannier, R. N., Hildebrandt, L., Lagergren, C., et al. (2011). Gadolinia-doped ceria mixed with alkali carbonates for solid oxide fuel cell applications: I. A thermal, structural and morphological insight. *J. Power Sources* 196 (13), 5546–5554. doi:10.1016/j.jpowsour.2011.02.004

Demin, A. K., and Bronin, D. I. (2023). Solid state electrochemical devices for hydrogen energy. *Electrochem. Mater. Technol.* 2 (2), 20232016. doi:10.15826/elmattech.2023.2.016

Gao, Y., Zhang, M., Fu, M., Hu, W., Tong, H., and Tao, Z. (2023). A comprehensive review of recent progresses in cathode materials for Proton-conducting SOFCs. *Energy Rev.* 2, 100038. doi:10.1016/j.enrev.2023.100038

Gordeev, E. V., and Porotnikova, N. M. (2023). Approaches for the preparation of dense ceramics and sintering aids for Sr/Mg doped lanthanum gallate: focus review. *Electrochem. Mater. Technol.* 2 (4), 20232022. doi:10.15826/elmattech.2023.2.022

Goulart, C. A., Boas, L. A. V., Morelli, M. R., and de Souza, D. P. F. (2021). Reactive sintering of yttrium-doped barium zirconate (BaZr0. 8Y0. 2O3-δ) without sintering aids. *Ceram. Int.* 47 (2), 2565–2571. doi:10.1016/j.ceramint.2020.09.102

Hanif, M. B., Rauf, S., Mosiałek, M., Khan, K., Kavaliukė, V., Kežionis, A., et al. (2023b). Mo-doped BaCe0· 9Y0· 1O3-δ proton-conducting electrolyte at intermediate temperature SOFCs. Part I: microstructure and electrochemical properties. *Int. J. Hydrogen Energy*. doi:10.1016/j.ijhydene.2023.01.144

Hanif, M. B., Rauf, S., Motola, M., Babar, Z. U. D., Li, C.-J., and Li, C.-X. (2022). Recent progress of perovskite-based electrolyte materials for solid oxide fuel cells and performance optimizing strategies for energy storage applications. *Mater. Res. Bull.* 146, 111612. doi:10.1016/j.materresbull.2021.111612

Hanif, M. B., Rauf, S., ul Abadeen, Z., Khan, K., Tayyab, Z., Qayyum, S., et al. (2023a). Proton-conducting solid oxide electrolysis cells: relationship of composition-structure-property, their challenges, and prospects. *Matter* 6 (6), 1782–1830. doi:10.1016/j.matt.2023.04.013

Hossain, M. K., Biswas, M. C., Chanda, R. K., Rubel, M. H., Khan, M. I., and Hashizume, K. (2021a). A review on experimental and theoretical studies of perovskite barium zirconate proton conductors. *Emergent Mater.* 4, 999–1027. doi:10.1007/s42247-021-00230-5

Hossain, M. K., Chanda, R., El-Denglawey, A., Emrose, T., Rahman, M. T., Biswas, M. C., et al. (2021b). Recent progress in barium zirconate proton conductors for electrochemical hydrogen device applications: a review. *Ceram. Int.* 47 (17), 23725–23748. doi:10.1016/j.ceramint.2021.05.167

Huang, J., Gao, Z., and Mao, Z. (2010). Effects of salt composition on the electrical properties of samaria-doped ceria/carbonate composite electrolytes for low-temperature SOFCs. *Int. J. Hydrogen Energy* 35 (9), 4270–4275. doi:10.1016/j.ijhydene.2010.01.063

Irshad, M., Baber, K., Hanif, M. B., Asad, M., Ghaffar, A., Rafique, M., et al. (2023). Synergistic role of Biomolecules and Bio-chelating agents in the sustainable development of an efficient BaCe0. 97M0. 03O3-δ (M= Sm, Gd) perovskite electrolyte for IT-SOFC. *Ceram. Int.* 49, 38360–38366. doi:10.1016/j.ceramint.2023.09.170

Irshad, M., Khalid, M., Rafique, M., Tabish, A. N., Shakeel, A., Siraj, K., et al. (2021). Electrochemical investigations of BaCe0. 7-xSmxZr0. 2Y0. 1O3-δ sintered at a low sintering temperature as a perovskite electrolyte for IT-SOFCs. *Sustainability* 13 (22), 12595. doi:10.3390/su132212595

Irshad, M., Kousar, N., Hanif, M. B., Tabish, A. N., Ghaffar, A., Rafique, M., et al. (2022). Investigating the microstructural and electrochemical performance of novel La

0.3 Ba 0.7 Zr 0.5 X 0.3 Y 0.2 (X= Gd, Mn, Ce) electrolytes at intermediate temperature SOFCs. *Sustain. Energy and Fuels* 6 (23), 5384–5391. doi:10.1039/d2se01147f

Irshad, M., Siraj, K., Raza, R., Ali, A., Tiwari, P., Zhu, B., et al. (2016). A brief description of high temperature solid oxide fuel cell's operation, materials, design, fabrication technologies and performance. *Appl. Sci.* 6 (3), 75. doi:10.3390/app6030075

Ji, H. I., Kim, B. K., Son, J. W., Yoon, K. J., and Lee, J. H. (2021). Influence of sintering activators on electrical property of BaZr0. 85Y0. 15O3-δ proton-conducting electrolyte. *J. Power Sources* 507, 230296. doi:10.1016/j.jpowsour.2021.230296

Jiao, J., Li, Q., Gu, Y., Luo, Y., Ge, L., Zheng, Y., et al. (2019). Effect of BaOB2O3 composite sintering aid on sinterability and electrical property of BaZr0. 85Y0. 15O3-δ ceramic. *Ceram. Int.* 45 (11), 13679–13684. doi:10.1016/j.ceramint.2019.04.062

Jincy, C. S., and Meena, P. (2022). Evaluation of cytotoxic activity of Fe doped cobalt oxide nanoparticles. *J. Trace Elem. Med. Biol.* 70, 126916. doi:10.1016/j.jtemb.2021.126916

Khan, K., Qayyum, S., Hanif, M. B., Rauf, S., Sultan, A., Mosiałek, M., et al. (2023). Design of efficient and durable symmetrical protonic ceramic fuel cells at intermediate temperatures via B-site doping of Ni in BaCe0. 56Zr0. 2Ni0. 04Y0. 2O3–δ. *Ceram. Int.* 49 (11), 16826–16835. doi:10.1016/j.ceramint.2023.02.043

Mehran, M. T., Khan, M. Z., Song, R. H., Lim, T. H., Naqvi, M., Raza, R., et al. (2023). A comprehensive review on durability improvement of solid oxide fuel cells for commercial stationary power generation systems. *Appl. Energy* 352, 121864. doi:10.1016/j.apenergy.2023.121864

Mosiałek, M., Hanif, M. B., Šalkus, T., Kežionis, A., Kazakevičius, E., Orliukas, A. F., et al. (2023). Synthesis of Yb and Sc stabilized zirconia electrolyte (Yb0. 12Sc0. 08Zr0. 8O2–δ) for intermediate temperature SOFCs: microstructural and electrical properties. *Ceram. Int.* 49 (10), 15276–15283. doi:10.1016/j.ceramint.2023.01.111

Nayak, A. K., and Sasmal, A. (2023). Recent advance on fundamental properties and synthesis of barium zirconate for proton conducting ceramic fuel cell. *J. Clean. Prod.* 386, 135827. doi:10.1016/j.jclepro.2022.135827

Osinkin, D. A. (2023). Some aspects of hydrogen oxidation in solid oxide fuel cell: a brief historical overview. *Electrochem. Mater. Technol.* 2 (3), 20232018. doi:10.15826/elmattech.2023.2.018

Park, K. Y., Seo, Y., Kim, K. B., Song, S. J., Park, B., and Park, J. Y. (2015). Enhanced proton conductivity of yttrium-doped barium zirconate with sinterability in protonic ceramic fuel cells. *J. Alloys Compd.* 639, 435–444. doi:10.1016/j.jallcom.2015.03.168

Pikalova, E. Y., Kalinina, E. G., and Pikalova, N. S. (2023). Recent advances in electrophoretic deposition of thin-film electrolytes for intermediate-temperature solid oxide fuel cells. *Electrochem. Mater. Technol.* 2 (1), 20232011. doi:10.15826/elmattech.2023.2.011

Rafique, M., Safdar, N., Irshad, M., Usman, M., Akhtar, M., Saleem, M. W., et al. (2022). Influence of low sintering temperature on BaCe0. 2Zr0. 6Y0. 2O3– δ IT-SOFC perovskite Electrolyte synthesized by Co-precipitation method. *Materials* 15 (10), 3585. doi:10.3390/ma15103585

Rasaki, S. A., Liu, C., Lao, C., and Chen, Z. (2021). A review of current performance of rare earth metal-doped barium zirconate perovskite: the promising electrode and electrolyte material for the protonic ceramic fuel cells. *Prog. Solid State Chem.* 63, 100325. doi:10.1016/j.progsolidstchem.2021.100325

Rauf, S., Hanif, M. B., Wali, F., Tayyab, Z., Zhu, B., Mushtaq, N., et al. (2023). Highly active interfacial sites in SFT-SnO₂ heterojunction electrolyte for enhanced fuel cell performance via engineered energy bands: envisioned theoretically and experimentally. *Energy and Environ. Mater.* 23, e12606. doi:10.1002/eem2.12606

Rehman, S. U., Shaur, A., Kim, H. S., Joh, D. W., Song, R. H., Lim, T. H., et al. (2021). Effect of transition metal doping on the sintering and electrochemical properties of GDC buffer layer in SOFCs. *Int. J. Appl. Ceram. Technol.* 18 (2), 511–524. doi:10.1111/ijac.13650

Shaheen, I., Hussain, I., Zahra, T., Javed, M. S., Shah, S. S. A., Khan, K., et al. (2023). Recent advancements in metal oxides for energy storage materials: design, classification, and electrodes configuration of supercapacitor. *J. Energy Storage* 72, 108719. doi:10.1016/j.est.2023.108719

Soares, H. S., Antunes, I., Loureiro, F. J., Pérez-Coll, D., Willinger, M. G., Brandão, A. D., et al. (2021). Effect of the addition mechanism of ZnO sintering aid on densification, microstructure and electrical properties of Ba (Zr, Y) O3-δ proton-conducting perovskite. *Int. J. Hydrogen Energy* 46 (52), 26466–26477. doi:10.1016/j.ijhydene.2021.05.109

Tao, S., and Irvine, J. T. (2007). Conductivity studies of dense yttrium-doped BaZrO3 sintered at 1325 C. *J. Solid State Chem.* 180 (12), 3493–3503. doi:10.1016/j.jssc.2007.09.027

Tarasova, N., Hanif, M. B., Janjua, N. K., Anwar, S., Motola, M., and Medvedev, D. (2023). Fluorine-insertion in solid oxide materials for improving their ionic transport and stability. A brief review. *Int. J. Hydrogen Energy* 23, 74. doi:10.1016/j.ijhydene.2023.08.074

Tong, H., Fu, M., Yang, Y., Chen, F., and Tao, Z. (2022). A novel self-assembled cobalt-free perovskite composite cathode with triple-conduction for intermediate proton-conducting solid oxide fuel cells. *Adv. Funct. Mater.* 32 (48), 2209695. doi:10.1002/adfm.202209695

Ueno, K., Hatada, N., Han, D., and Uda, T. (2019). Thermodynamic maximum of Y doping level in barium zirconate in co-sintering with NiO. *J. Mater. Chem. A* 7 (12), 7232–7241. doi:10.1039/c8ta12245h

Uthayakumar, A., Pandiyan, A., Mathiyalagan, S., Keshri, A. K., and Krishna Moorthy, S. B. (2020). The effect of space charge on blocking grain boundary resistance in an yttrium-doped barium zirconate electrolyte for solid oxide fuel cells. *J. Phys. Chem. C* 124 (10), 5591–5599. doi:10.1021/acs.jpcc.0c00166

Uwah, E. I., Ndahi, N. P., Abdulrahman, F. I., and Ogugbuaja, V. O. (2011). Heavy metal levels in spinach (Amaranthus caudatus) and lettuce (Lactuca sativa) grown in Maiduguri, Nigeria. *J. Environ. Chem. Ecotoxicol.* 3 (10), 264–271.

Vera, C. Y. R., Ding, H., Peterson, D., Gibbons, W. T., Zhou, M., and Ding, D. (2021). A mini-review on proton conduction of BaZrO3-based perovskite electrolytes. *J. Phys. Energy* 3 (3), 032019. doi:10.1088/2515-7655/ac12ab

Xie, H., Wei, Z., Yang, Y., Chen, H., Ou, X., Lin, B., et al. (2018). New Gd-Zn co-doping enhanced mechanical properties of BaZrO3 proton conductors with high conductivity for IT-SOFCs. *Mater. Sci. Eng. B* 238, 76–82. doi:10.1016/j.mseb.2018.12.012

Zhang, W., and Hu, Y. H. (2021). Progress in proton-conducting oxides as electrolytes for low-temperature solid oxide fuel cells: from materials to devices. *Energy Sci. Eng.* 9 (7), 984–1011. doi:10.1002/ese3.886

Zheng, Y., Yang, C., Pu, W., and Zhang, J. (2009). Determination of oxalic acid in spinach with carbon nanotubes-modified electrode. *Food Chem.* 114 (4), 1523–1528. doi:10.1016/j.foodchem.2008.11.021